



Development of the adjoint of the unified tropospheric–stratospheric chemistry extension (UCX) in GEOS-Chem adjoint v36

Irene C. Dedoussi^{1,2,3}, Daven K. Henze⁴, Sebastian D. Eastham^{3,5}, Raymond L. Speth³, and Steven R. H. Barrett³

¹Section Aircraft Noise and Climate Effects, Faculty of Aerospace Engineering, Delft University of Technology, Kluyverweg 1, 2629 HS, Delft, the Netherlands

²Department of Engineering, University of Cambridge, 1 JJ Thomson Ave, Cambridge, CB3 0DY, United Kingdom

³Laboratory for Aviation and the Environment, Department of Aeronautics and Astronautics, Massachusetts Institute of Technology, 77 Massachusetts Avenue, Cambridge, MA 02139, United States

⁴Department of Mechanical Engineering, University of Colorado Boulder, 1111 Engineering Drive, Boulder, CO 80309, United States

⁵Department of Aeronautics, Imperial College London, South Kensington Campus, London, SW7 2AZ, United Kingdom

Correspondence: Irene C. Dedoussi (icd23@cam.ac.uk)

Received: 3 December 2023 – Discussion started: 23 January 2024

Revised: 17 April 2024 – Accepted: 4 May 2024 – Published: 30 July 2024

Abstract. Atmospheric sensitivities (gradients), quantifying the atmospheric response to emissions or other perturbations, can provide meaningful insights on the underlying atmospheric chemistry or transport processes. Atmospheric adjoint modeling enables the calculation of receptor-oriented sensitivities of model outputs of interest to input parameters (e.g., emissions), overcoming the numerical cost of conventional (forward) modeling. The adjoint of the GEOS-Chem atmospheric chemistry–transport model is a widely used such model, but prior to v36 it lacked extensive stratospheric capabilities. Here, we present the development and evaluation of the discrete adjoint of the global chemistry–transport model (CTM) GEOS-Chem unified chemistry extension (UCX) for stratospheric applications, which extends the existing capabilities of the GEOS-Chem adjoint to enable the calculation of sensitivities that include stratospheric chemistry and interactions. This development adds 37 new tracers, 273 kinetic and photolysis reactions, an updated photolysis scheme, treatment of stratospheric aerosols, and all other features described in the original UCX paper. With this development the GEOS-Chem adjoint model is able to capture the spatial, temporal, and speciated variability in stratospheric ozone depletion processes, among other processes. We demonstrate its use by calculating 2-week sensitivities of stratospheric ozone to precursor species and show that the adjoint captures the Antarctic ozone depletion potential of active halo-

gen species, including the chlorine activation and deactivation process. The spatial variations in the sensitivity of stratospheric ozone to NO_x emissions are also described. This development expands the scope of research questions that can be addressed by allowing stratospheric interactions and feedbacks to be considered in the tropospheric sensitivity and inversion applications.

1 Introduction

Chemistry–transport models (CTMs) that simulate the chemistry, transport, and deposition processes in the atmosphere provide a tool to investigate the atmospheric impact of current emissions, as well as emissions scenarios resulting from technological or policy decisions. Global CTMs that simulate both the troposphere and the stratosphere (and capture interactions between the two) can be employed to calculate stratospheric ozone, which plays a critical role in absorbing incoming solar ultraviolet (UV) light that could otherwise be harmful to human health, animals, plants, biogeochemistry, air quality, and materials (WMO/UNEP, 2014). Examples of such are the GEOS-Chem UCX (unified tropospheric–stratospheric chemistry extension; Eastham et al., 2014), MOZART-3 (Kinnison et al., 2007), TM5 (Huijnen et al., 2010), GMI (Consideine et al., 2000; Rotman et al., 2001),

OSLO-CTM3 (Søvde et al., 2012), and EMAC (Sausen et al., 2010). GEOS-Chem is a 3D global CTM originally developed by Bey et al. (2001) and updated (<http://www.geos-chem.org>, last access: 16 July 2024) with the unified chemistry extension (UCX) (Eastham et al., 2014). It has been used to quantify a variety of ozone-related mechanisms and impacts including those of aviation-related ozone (Eastham and Barrett, 2016; Quadros et al., 2020), stratospheric ozone intrusions (Greenslade et al., 2017), and accelerated stratospheric ozone loss (Eastham et al., 2018), as well as processes of other atmospheric constituents such as halogens (Wang et al., 2019; Zhu et al., 2019; Sherwen et al., 2016).

The atmospheric parameters that affect and control the behavior of the ozone layer can be assessed through sensitivity analyses. As explained by Hakami et al. (2007) and Clappier et al. (2017), sensitivity analyses can be performed in a forward or backward (adjoint) manner. In the forward method, a perturbation is introduced in a parameter of interest (source), and sensitivities are propagated from the perturbed source into the various receptors/outputs. The methods in this category (one of which is finite difference, also known as “brute force”) are efficient in simultaneously providing information about all receptors with respect to the perturbed parameter. This method, however, is constrained by numerical noise (e.g., cancellation errors) (Hakami et al., 2007). When assessing the impacts of various sources, this approach can also result in significant computational overhead. In the backward (or adjoint) sensitivity analysis, a perturbation in the receptor is propagated backwards in time and space through an auxiliary set of equations, thus linking the effect on a scalar model output (receptor) originating from multiple model parameters (sources). As a result, the adjoint sensitivity analysis provides simultaneous sensitivity information about a specific outcome with respect to all sources and parameters. For example, an adjoint evaluation could provide, in a single simulation, the effect of perturbations of any ozone precursor species at any location in the computational domain on the total global stratospheric ozone mass. Adjoint sensitivity analyses can also be used with gradient-based optimization algorithms (e.g., 4D-Var) to optimize model parameters and inputs (Kopacz et al., 2010; Qu et al., 2020).

The adjoint of the GEOS-Chem CTM was developed by Henze et al. (2007) with several updates since (Capps et al., 2012; Gu et al., 2023; Tang et al., 2023; Wang et al., 2012, and others). Although having extensive tropospheric chemistry capabilities, prior to v36 stratospheric processes were calculated based on archived data or simplified parameterizations (similar to the GEOS-Chem model capabilities before the introduction of the UCX). Stratospheric ozone is calculated using the linearized ozone parameteriza-

tion (Linoz) scheme (Singh et al., 2009). The evolution of most other species in the stratosphere is calculated from production and loss rates archived from NASA’s Global Modeling Initiative (GMI) code (Murray et al., 2012; Rotman et al., 2001). Finally, given that v35 of the adjoint of GEOS-Chem is troposphere-focused, tracers necessary for detailed stratospheric calculations (e.g., chlorofluorocarbons (CFCs), water, and methane) and processes (including stratospheric aerosols, polar stratospheric clouds, emissions from long-lived species) are also not present in pre-UCX versions.

Stratospheric processes and impacts however represent a crucial component of atmospheric chemistry, necessitating models to be able to quantify them and better understand them. Ozone has direct effects on human health, with exposure to UV light leading to an increased likelihood of eye damage and/or skin cancer (Slaper et al., 1996). After the discovery of the ozone-depleting effect of industrially produced CFCs and halons over the Antarctic (“ozone hole”) as well as significant losses in other latitudes, the nations of the world agreed to protect the ozone layer under the 1987 Montreal Protocol and its amendments (Farman et al., 1985; Molina and Rowland, 1974; Solomon, 1999; McElroy et al., 1986; Solomon et al., 1986). In addition to CFCs, high-altitude emissions (including volcanic emissions), climate change, and sunlight affect stratospheric ozone and need to be considered in modeling of stratospheric chemistry. While the Antarctic ozone hole has shown signs of recovery, the ozone layer remains an environmental topic of discussion (Ball et al., 2018; Solomon et al., 2016; Kuttippurath and Nair, 2017), as technological changes, industrial chemicals, and climate change could have a direct effect on stratospheric ozone depletion. There has been recent interest in supersonic commercial aircraft that cruise at $\sim 50\,000$ ft, emitting nitrogen oxides (NO_x), which are also known to contribute to ozone depletion (Johnston, 1971; Crutzen, 1970; Cunnold et al., 1977; Eastham et al., 2022). Further, high-altitude aviation emissions are known to change the ozone vertical distribution in the atmosphere (Eastham and Barrett, 2016; Köhler et al., 2008; Emmons et al., 2012; Brasseur et al., 1998; Maruhashi et al., 2022). Aviation emissions and corresponding impacts are expected to increase given that aviation is the transportation sector with the highest growth rate, with no direct replacement alternative (Schäfer et al., 2009). In addition, an increasing number of rocket launches and associated re-entry payloads could also lead to higher emissions at stratospheric levels (Ross et al., 2009; Ryan et al., 2022). Industrial chemicals, in the form of short-lived chlorine species not controlled by the Montreal Protocol, have also been highlighted in terms of their ozone depletion potential (Hossaini et al., 2015, 2017). At the same time, CFC-11 and CFC-12 emissions, controlled by the Montreal Protocol, are found to be unexpectedly increasing (Rigby et al., 2019; Lickley et al., 2020; Montzka et al., 2018). Finally, the projected cooling of the stratosphere under increased greenhouse gas emission scenarios could affect ozone depletion potentials and thereby

the recovery of the ozone hole (Weatherhead and Andersen, 2006).

In this paper we describe an alternative way of quantifying the effects of perturbations in ozone-depleting precursors through the development of the adjoint of GEOS-Chem UCX, which is the first adjoint model of a unified tropospheric–stratospheric detailed chemistry–transport model. The paper is structured as follows: Sect. 2 describes the UCX model and its adjoint development, and Sect. 3 provides the model evaluation. Section 4 presents an application of the newly developed capabilities, computing sensitivities of stratospheric ozone burden to ozone-depleting precursor perturbations in the global domain. Section 5 summarizes the paper and lists limitations of the model development and application.

2 Methods

An adjoint model consists of a base (“forward component”) model and its corresponding differentiated counterpart (“differentiated component”). The forward model on which the GEOS-Chem adjoint is based corresponds to GEOS-Chem v8-02-01 with several updates and bug fixes, whereas the GEOS-Chem UCX forward model is version v10-01. The development in this work entails first updating the forward component in the adjoint to match the GEOS-Chem UCX capabilities in v10-01 and subsequently developing the corresponding differentiated counterpart code. The capabilities of the forward UCX model that are incorporated into the forward component of the adjoint are outlined in Sect. 2.1 below. The development choices for the adjoint model are then described in Sect. 2.2.

2.1 The UCX model

The GEOS-Chem UCX, as described and validated by Eastham et al. (2014), introduced stratospheric capabilities to the global GEOS-Chem CTM, without compromising the existing tropospheric capabilities. This section briefly details the implementation of the UCX into the forward component of the GEOS-Chem adjoint, in addition to auxiliary changes required for the UCX capabilities to function.

The vertical domain of the chemical solver is extended to the top of the stratosphere, corresponding to ~ 1 hPa or ~ 50 km, and the vertical resolution in the stratosphere is increased to match that of the GEOS model. This corresponds to an additional ~ 30 vertical layers, resulting in full chemistry calculations being solved in 59 of the 72 total vertical grid layers. A total of 37 new tracers, necessary for the stratospheric chemistry calculations, are added to the GEOS-Chem adjoint model and are listed in Table S1 of the Supplement. These also include water vapor and methane, which are now chemically active species within the model. Surface mixing ratio boundary conditions are added for the newly in-

troduced long-lived species. The existing Fast-J photolysis scheme did not consider wavelengths shorter than 289 nm, since those wavelengths are attenuated above the tropopause (Bian and Prather, 2002). These wavelengths however are essential in stratospheric chemistry (Sander et al., 2000). The photolysis scheme is thus updated to Fast-JX v7.0, which expands the spectrum analyzed to 18 wavelength bins covering 177–850 nm and extends the upper altitude limit to approximately 60 km (Bian and Prather, 2002; Eastham et al., 2014). We add 217 kinetic reactions and 43 photolytic decomposition processes to bring the existing chemical mechanism in the GEOS-Chem adjoint up to speed with the UCX forward model mechanism. The original UCX additions were designed to match the GMI stratospheric chemistry mechanism (Rotman et al., 2001) and to update the rates to JPL10-06 (Sander et al., 2011). We use the Kinetic PreProcessor (KPP) software library, version 2.2.3, to automatically generate the chemical mechanism (Damian et al., 2002; Sandu et al., 2003; Daescu et al., 2003) and include it in the model. Polar stratospheric cloud-related reactions are also added. For a complete description of the GEOS-Chem UCX module we refer to Eastham et al. (2014). Other minor additions, including mesospheric H_2SO_4 photolysis and mesospheric NO_x and N_2O loss rates and bug fixes introduced since the release of UCX, are also added. Finally, we make no changes to global transport, convection, or mixing processes. Each individual change introduced is evaluated against the forward model (where possible). The entire model evaluation is described in Sect. 3.1.

2.2 Model development

To calculate adjoint sensitivities (gradients), the differentiated model needs to be generated from the base (forward component) model. Adjoint code can be derived in two ways: continuous and discrete. In a continuous adjoint, the model governing equations are differentiated and then discretized for numerical solution. In such a case, the adjoint equations maintain their physical interpretability, but the algorithmic treatment may be very different from the forward component. In a discrete adjoint, the already discretized forward component is differentiated directly. Sandu et al. (2005) provide a description of discrete and continuous adjoints of CTMs.

The GEOS-Chem UCX algorithm is inherently discretized (e.g., heterogeneous chemistry regimes), and there are therefore discontinuities in the algorithm. The discrete adjoint approach overcomes the difficulty of branching and other discontinuities (if statements, max/min values, goto) by generating corresponding code for each branch and thus allowing direct validation across multiple regimes. In this work a discrete adjoint approach is selected for the UCX adjoint, as it allows us to maintain algorithmic consistency with the GEOS-Chem UCX and thereby enables direct validation.

Following the discrete adjoint approach entails generating the adjoint model (differentiated component) of the dis-

cretized forward component code. This is done through a combination of manually (by hand) derived and automatically generated differentiated code using the Tapenade automatic differentiation (AD) tool (Hascoet and Pascual, 2013; Giering and Kaminski, 1998). Tapenade provides analytical derivatives of the computer program functions in cases where there is significant variable interdependence and length of code. Using AD requires some prior manipulation of the input code and additional manual manipulation of the generated code to incorporate it in the adjoint model. The decision between deriving the adjoint code manually and using AD tools usually depends on the length and complexity of the individual (sub-)routine or process. The adjoint of the chemistry mechanism is directly generated through KPP (Damian et al., 2002; Sandu et al., 2003; Daescu et al., 2003).

Since the adjoint model is integrated backwards in time, intermediate values from the forward model variables (e.g., concentrations) are required (Zhao et al., 2020). This is usually referred to as checkpointing, and for this we follow a consistent approach with the rest of the GEOS-Chem adjoint model. Specifically, during the forward model calculation, these are saved at specific external time steps in checkpoint files during the forward calculation, and intermediate values required are recalculated as needed. The PUSH/POP functions of Tapenade are utilized to store and retrieve (in reverse) recomputed forward model variable values that are needed in the adjoint equations. This approach balances the trade-offs between storage, memory, and CPU (Henze et al., 2007).

In a model evaluation context, adjoint sensitivities are typically compared to finite difference sensitivities due to their ease of calculation, although potential errors introduced due to round-off, nonlinear effects, and discontinuities must be considered (Capps et al., 2012; Giles and Pierce, 2000). Each individual adjoint subroutine is independently evaluated against forward model sensitivities. The entire adjoint model evaluation is described in Sect. 3.2.

3 Model evaluation

First the implemented UCX model in the GEOS-Chem adjoint forward component is evaluated against the stand-alone GEOS-Chem UCX model. This evaluation is described in Sect. 3.1. Sensitivities from the differentiated counterpart of the adjoint model are then evaluated against finite-difference-based sensitivities from the forward model component. This evaluation is described in Sect. 3.2.

3.1 Base (forward component) model evaluation

To evaluate the performance of the forward model extensions in the GEOS-Chem adjoint model, we perform a 5-year-long simulation (1 January 2008–1 January 2013). The mean age of air in the upper stratosphere is approximately

5 years, measured from stratospheric entry at the tropical tropopause, and is thereby a sufficiently long time to test whether the stratospheric cycle is represented accurately in the model (Butchart, 2014). We perform three such simulations: one for the stand-alone GEOS-Chem UCX model (validated in Eastham et al., 2014), one for the forward component of the GEOS-Chem adjoint v35f before the introduction of the UCX capabilities, and one for the forward component of the GEOS-Chem adjoint with the newly introduced UCX extensions. The global grid has a horizontal resolution of $4^\circ \times 5^\circ$ latitude and longitude, respectively, and 72 vertical hybrid sigma–eta pressure levels extending from the surface to 0.01 hPa. The model is driven by GEOS-5 meteorological fields from the Global Modeling and Assimilation Office (GMAO) at the NASA Goddard Space Flight Center. Identical initial conditions are used for all simulations. These are obtained by running the stand-alone GEOS-Chem UCX model for a 3-year time period (prior to the 5-year simulation) to “spin up” the model. Long-lived species are initialized based on archived zonal-mean mixing ratios from the 2D stratospheric model AER CTM (Weisenstein et al., 1997).

Figure 1 shows the zonal-mean column ozone (in Dobson units) for the 5-year-long run for the forward UCX model, the forward component of the adjoint model (“pre-UCX” adjoint), and the forward component of the UCX adjoint model (developed as part of this work), shown in the top, middle, and bottom panels, respectively. Due to tracer differences between the models, O_3 is used for the forward UCX model and O_x for the adjoint forward components. However, we note that the openly available v36 now uses O_3 as a tracer instead of O_x (in addition to NO and NO_2 instead of NO_x). Similar to Eastham et al. (2014), we use the ozone layer to demonstrate the improved stratospheric modeling, as it is a key feature of the stratosphere and sensitive to a variety of stratospheric processes (e.g., halogen cycles, aerosol formation, short-wavelength photochemistry). First, we are able to reliably reproduce the behavior at mid-latitudes using online chemistry – this was achieved through relaxation to a known climatology in the pre-UCX adjoint forward component. This is also evident in Fig. 2, which shows the mean ozone column as a function of latitude for 2010 for the three model versions. Second, the Antarctic ozone seasonal cycle, a feature not captured in the “pre-UCX” adjoint forward component, is now replicated (as in the standalone UCX model). This is characterized by the formation of a deep “ozone hole” each September and the subsequent recovery by the end of the year (Solomon, 1999). This influences the rest of the Southern Hemisphere after the breakdown of the polar vortex each spring (Eastham et al., 2014). The mean zonal averaged absolute column ozone difference between the UCX standalone model and the UCX adjoint forward component is 2.7 % for the 5-year run. Besides ozone, other key species have been compared, with the example of NO_x included in the Supplement. These differences are to be expected as the UCX standalone model includes additional

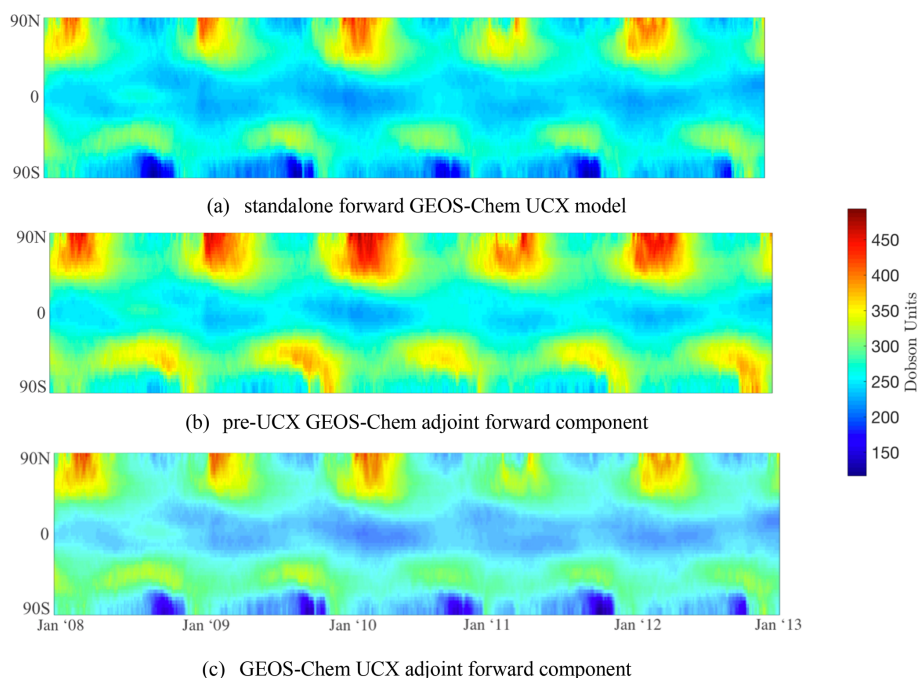


Figure 1. Zonal-mean column ozone for 2008–2012 from the standalone forward GEOS-Chem UCX model (a), the pre-UCX GEOS-Chem adjoint base (forward component) model (b), and the GEOS-Chem UCX adjoint the base (forward component) model (c). O_3 is shown for the forward UCX model and O_x for the adjoint forward components.

model updates and changes, beyond the UCX, that are not implemented in the adjoint forward component model.

3.2 Adjoint model evaluation

The choice of a discrete adjoint allows the evaluation of the adjoint sensitivities directly against the forward component code (Giles and Pierce, 2000). While the performance of the adjoint UCX model has been evaluated in a component-wise manner for each individual module change or introduction (see Supplement Table S2 for the module list), here we evaluate the adjoint model as a whole for the generation of short-term sensitivities. To assess the accuracy of the adjoint modules constructed, adjoint sensitivities are compared with finite difference sensitivities from the forward component at the end of a single chemistry time step (1 h). To overcome the different nature of finite difference and adjoint sensitivities (source- and receptor-oriented, respectively), transport and convection processes are disabled so that each column of the 3D grid acts independently. This way N evaluations are performed simultaneously, where N is the number of grid cells in each layer of the horizontal grid ($N = 46 \times 72$). In this column model test, the sensitivity of odd oxygen (O_x) mass with respect to NO_x mass is calculated. We choose the NO_x to O_x relationship as a way of evaluating the model given its central role in multiple atmospheric chemical pathways in both the stratosphere and the troposphere. This column model test is considered appropriate as no changes have

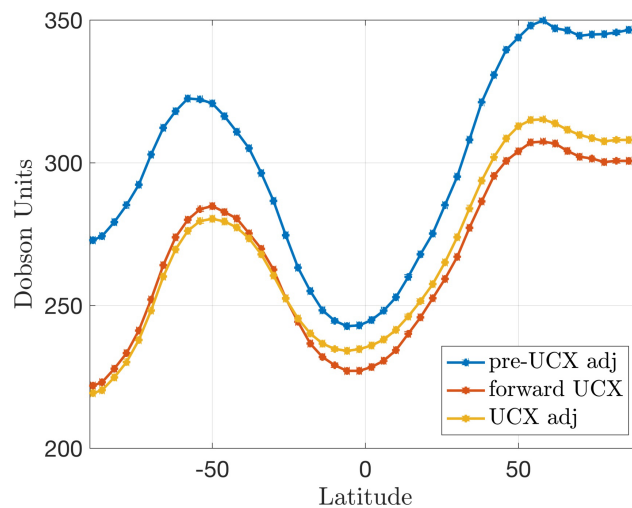


Figure 2. Mean column ozone for 2010 for the standalone forward GEOS-Chem UCX model (red), the pre-UCX GEOS-Chem adjoint base (forward component) model (blue), and the GEOS-Chem UCX adjoint base (forward component) model (yellow).

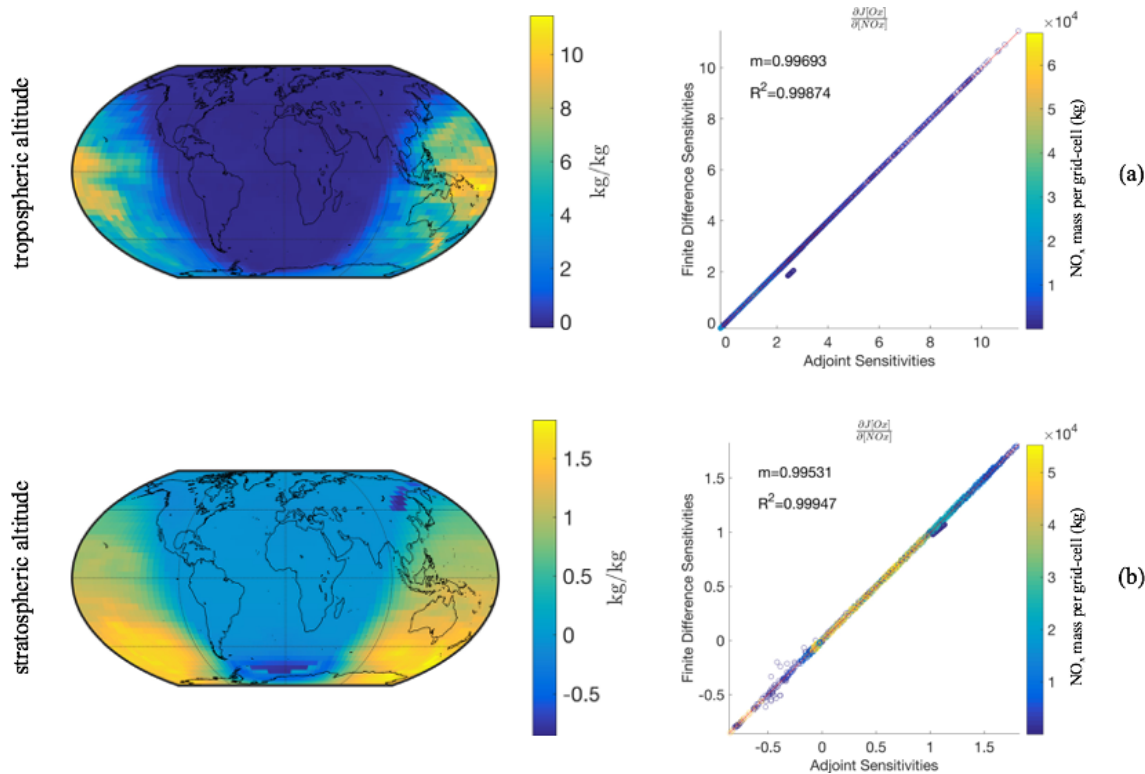


Figure 3. Adjoint model evaluation after a single chemistry time step (1 h) with disabled transport and convection processes. In the left column the adjoint sensitivities depict changes in O_x mass for NO_x perturbations in the same grid cell. In the right column are the adjoint gradients compared to finite difference gradients, with the corresponding linear regression slope, m , and coefficient of determination, R^2 , for all N column models tested simultaneously ($N = 46 \times 72$). Each point on the parity plot is colored according to the NO_x mass in the grid cell. Top row (a) shows a tropospheric model layer (4 km), and bottom row (b) shows a stratospheric model layer (21 km).

been introduced to the global transport, convection, or mixing processes. Overall, with the column model test we evaluate sensitivities obtained from the newly developed adjoint model against finite difference sensitivities from the forward GEOS-Chem (base) model for a variety of chemical conditions in the troposphere and the stratosphere.

Forward model sensitivities, Λ , are obtained using the finite difference (brute force) method, with a single-sided finite difference equation:

$$\Lambda = \frac{J(x_0 + h) - J(x_0)}{h}, \quad (1)$$

where J is the objective (cost) function, x_0 is the baseline state of the model, and h is the perturbation size. We evaluate these sensitivities at a tropospheric altitude of 3.9 km (625 hPa – model layer 20) to ensure that the tropospheric adjoint function is maintained and at a stratospheric altitude of 21 km (44 hPa – model layer 40) to ensure the functioning of the stratospheric additions. The perturbation size, h , is chosen to balance the effects of the nonlinearity of the response and the numerical round-off effects. On the one hand, a large h may result in a deviation off the point at which the finite difference sensitivity is evaluated and, in the case of

a nonlinear response, provide an inaccurate estimate of the sensitivity. On the other hand, a small h may result in subtraction round-off errors.

Figure 3 presents the sensitivity comparisons for each point in the global domain for an h value of 100 and 300 kg per grid cell for the tropospheric and stratospheric layer, respectively. We find that these h values balance the numerical artifacts of nonlinearity and round-off error effects when calculating the finite difference sensitivity Λ . In both stratospheric and tropospheric objective functions the gradients agree with $R^2 > 0.998$, with points off the regression line representing highly nonlinear regimes. The off-diagonal cluster of points consists of the southernmost grid cell row. While this evaluation is performed on an individual chemistry time step with horizontal transport processes disabled, it allows the simultaneous evaluation of the sensitivities for a wide range of different background conditions, including varying NO_x levels (right column in Fig. 3).

The effects of the choice of perturbation size, h , for the tropospheric and the stratospheric sensitivity evaluations are presented in Fig. 4. The clusters of off-diagonal points, which drive the R^2 , move closer to the diagonal as h decreases, indicating that these off-diagonal points represent nonlinear

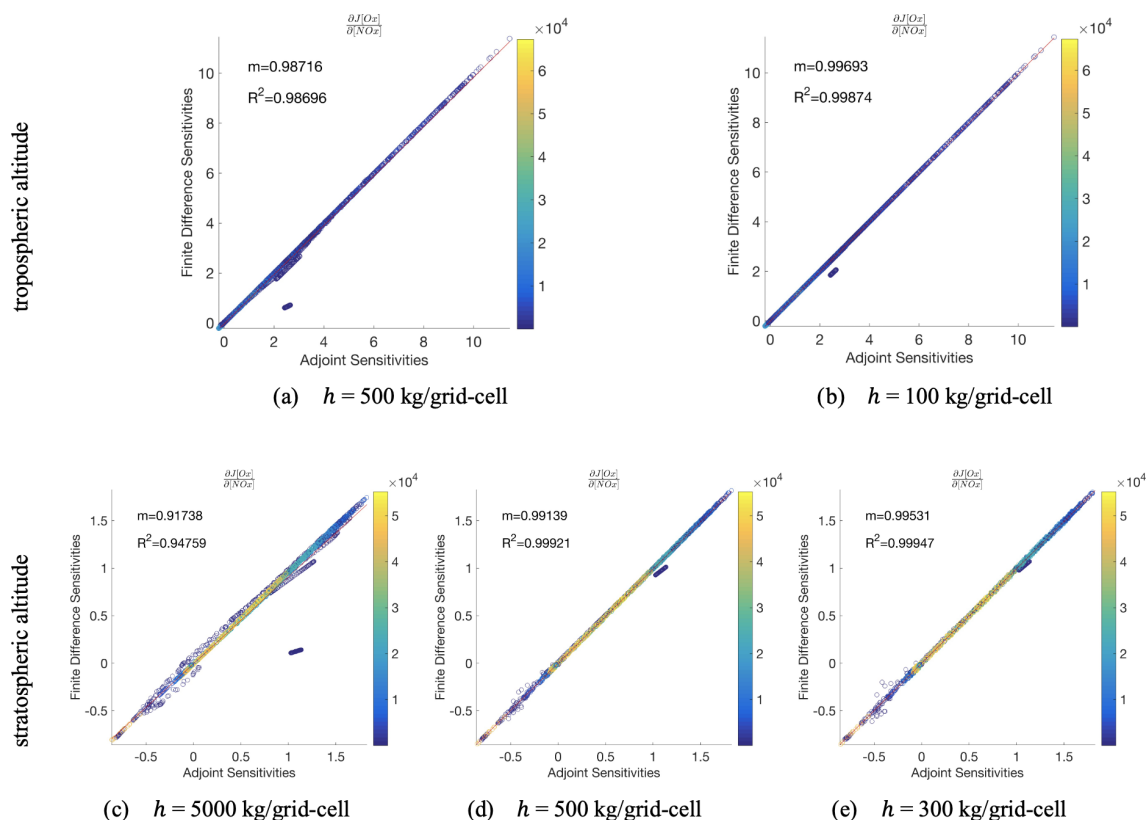


Figure 4. Adjoint model evaluation after a single chemistry time step (1 h) with disabled transport and convection processes for different NO_x perturbation sizes, h . Top row (panels a, b) displays the evaluation at a tropospheric model layer (4 km) and bottom row (panels c, d, e) at a stratospheric model layer (21 km). The adjoint gradients compared to finite difference gradients, with the corresponding linear regression slope, m , and coefficient of determination, R^2 , for all N column models tested simultaneously ($N = 46 \times 72$). Each point on the parity plot is colored according to the NO_x mass in the grid cell.

regimes in both the stratospheric and tropospheric comparison. At the same time however, we note more numerical noise for smaller h values. For example, in the stratospheric case (panels c–e) the smaller the h , the higher the R^2 (driven by a larger number of nonlinear points) but more numerical noise points are evident (for sensitivities < 0) compared to the cases with the larger h .

The base (forward component) model evaluation presented in Sect. 3.1, together with the component-level evaluation of the new/updated modules as well as the whole-model single time step column evaluations presented here of the differentiated counterpart, providing confidence in the correct implementation of the UCX adjoint development. While this is considered sufficient for the short-term sensitivity applications in stratospheric ozone described in the upcoming section, long-term sensitivity calculations would be necessary to capture the full effects of tropospheric–stratospheric exchanges. Additional changes necessary to enable long-term evaluations are described in Fritz et al. (2022).

4 Model application

Using the updated tropospheric–stratospheric capabilities of the GEOS-Chem adjoint, we calculate short-term (2-week) ozone sensitivities to ozone-depleting substances and precursors. An individual run of the GEOS-Chem UCX adjoint quantifies the relationship between model parameter perturbations and a scalar quantity of interest (objective function). Here we provide three examples that illustrate the information provided by the adjoint sensitivities, aiming to demonstrate the extended capabilities of the developed model to capture stratospheric ozone depletion and its potential for providing an alternative way of examining the underlying chemical processes. For the following simulations, we use the global $4^\circ \times 5^\circ$ global horizontal resolution (latitude \times longitude) and 72 hybrid sigma–eta pressure levels extending from the surface to 0.01 hPa, driven by the GEOS-5 assimilated meteorological data from the Global Modeling and Assimilation Office (GMAO) at the NASA Goddard Space Flight Center. We use the spun-up initial conditions referred to in Sect. 3.1 for each simulation, ensuring that the concentrations of species (including reservoir species)

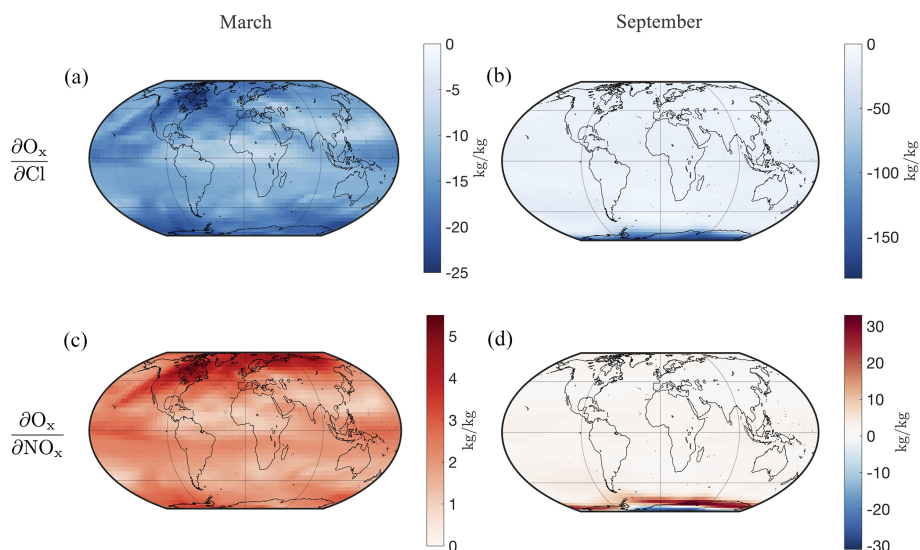


Figure 5. Sensitivities of aggregate O_x in a stratospheric vertical model layer (~ 21 km) with respect to perturbations in Cl (**a, b**) and in NO_x (**c, d**) mass in the global domain of the same model layer for a 2-week simulation. Panels (**a**) and (**c**) present these for 1–15 March and (**b**) and (**d**) for 1–15 September.

are spatially and temporally appropriate. We run the GEOS-Chem adjoint for 2-week intervals. This timescale is sufficient for capturing chemical relationships between ozone and short-term catalytic loss agents (e.g., active halogen and NO_x species) at the corresponding altitudes and times of the year. We perform the simulations for odd oxygen as an objective function (numerator of sensitivity), for 1–15 March and 1–15 September 2010, to capture the polar ozone depletion phenomena. We also use objective functions of stratospheric “activated” and “unreactive” chlorine to better describe the drivers behind the Antarctic ozone sensitivities calculated.

Figure 5 depicts the sensitivities of O_x at a stratospheric vertical layer of the model (layer 40) ranging between 20.9 and 22.0 km (47.6 and 40.2 hPa) with respect to perturbations in the NO_x and Cl mass at the same layer. Given the receptor-oriented nature of the adjoint method, the maps indicate how a perturbation in the NO_x and Cl mass anywhere in the domain would affect the aggregate O_x at the same vertical model layer (i.e., there is no spatial information on the resulting ozone changes). These are provided for March and September. During the Antarctic spring in September, the ozone depletion potential is highlighted, with ~ 5 times greater magnitude sensitivities of O_x to active chlorine (of which Cl is shown here), consistent with the observed high rates of heterogeneous chlorine activation during this period (Solomon, 1999). The sensitivities of O_x with respect to NO_x are also higher in absolute terms in September. Closer to the Antarctic the sign is negative, and surrounding the hole it is positive, reflecting the bounding of the hole over the Antarctic. We do not observe any sensitivity changes in the Arctic ozone in March. This may be due to an underestimate of Arctic ozone depletion by the forward model (see Fig. 1c) or due

to the higher variability in Arctic ozone depletion and the fact that 2010 was a relatively warm year in the Arctic with little NH polar cap ozone loss being observed (NASA Ozone Watch, 2018; Weber et al., 2018).

The September $\partial O_x/\partial NO_x$ and $\partial O_x/\partial Cl$ sensitivities are shown in an Antarctic stereographic projection in Fig. 6 (panels a and b, respectively), together with the corresponding O_x and $ClONO_2$ mixing ratios (panel c and d, respectively). The sensitivities are largely bounded inside the ozone “hole” (panel c). The rapid depletion of polar ozone which results in this ozone “hole” occurs due to catalytic cycles in the sunlit atmosphere driven by activated forms of chlorine (Solomon, 1999).

Chlorine, originating from compounds such as CFCs, exists at stratospheric altitudes in the form of inert reservoirs (e.g., $ClONO_2$ and HCl), referred to as “unreactive” chlorine. Following heterogeneous processes, unreactive chlorine can convert into more active forms of chlorine (e.g., Cl_2 , Cl, ClO, HOCl), referred to as “activated” or “reactive” chlorine. This partitioning of chlorine and the activation and deactivation processes are central for understanding the polar ozone depletion mechanism (Solomon et al., 2015).

We find a high $\partial O_x/\partial Cl$ sensitivity inside the ozone “hole” with a gradient towards the pole, illustrative of the odd chlorine catalytic cycle. In addition, the capability of NO_x to neutralize the available ClO (Cl shown as a proxy to ClO, since these cycle rapidly) into unreactive $ClONO_2$ varies from the pole to the edge of the ozone hole. Its sign reversal forming a positive sensitivity “collar” at the edge of the vortex links to the behavior of the Antarctic $ClONO_2$ “collar”, which is visible in Fig. 6d (Toon et al., 1989; Jaeglé et al., 1997; Chipperfield et al., 1994). Figure 7 shows the sensitivity of two chlo-

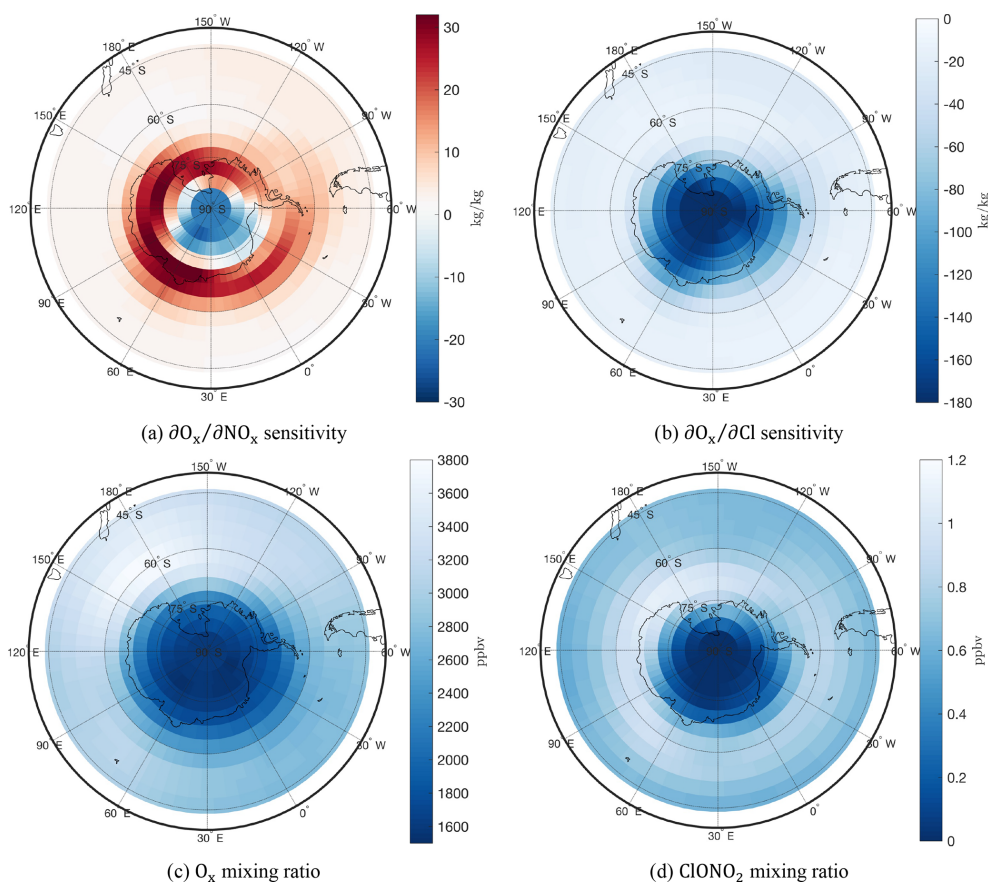


Figure 6. Stereographic plots of $\partial O_x/\partial NO_x$ (a) and $\partial O_x/\partial Cl$ (b) sensitivities in kg kg^{-1} , as well as O_x (c) and $ClONO_2$ (d) mixing ratios in ppbv, for a 2-week September simulation at a stratospheric vertical model layer (~ 21 km).

rine deactivation and activation pathways, $\partial ClONO_2/\partial NO_x$ and $\partial Cl_2/\partial HCl$, respectively. The deactivation “collar” in $\partial ClONO_2/\partial NO_x$ is likely the cause of the reversal in sign of the $\partial O_x/\partial NO_x$ sensitivity. The ozone loss, overlapping with the high chlorine activation region in Fig. 7b, is bounded over the Antarctic by this “collar” as active chlorine is converted back into the $ClONO_2$ unreactive reservoir.

Figure 8 shows the zonally averaged sensitivities of O_x mass at stratospheric altitudes between 20 and 30 km with respect to active halogen species mass, BrO and ClO, for the first 2 weeks of March and September 2010. Perturbations in ClO and BrO mass in all cases and at all altitudes lead to ozone depletion (negative sensitivity sign), reflecting the influence of catalytic halogen cycles (Solomon, 1999). As previously mentioned, no clear Arctic ozone depletion potential is obtained in this case, potentially due to the climatology that year. In the Antarctic region in September the sensitivities highlight the altitude and latitude area where the ozone hole appears. We note that the sensitivity of O_x with respect to BrO is ~ 15 times higher than the corresponding ClO one for both March and September on a per kilogram basis, in line with previous estimates of ~ 45 on a per atom basis (Daniel et al., 1999).

The receptor-oriented adjoint sensitivities allow us to examine relationships between ozone and its precursors by quantifying the effects of perturbations at different locations in the atmosphere. Given the interest in high-altitude NO_x perturbations from the potential re-introduction of supersonic civil aircraft, Fig. 9 shows zonally averaged sensitivities with objective functions of O_x at 10–20 and 20–30 km with respect to NO_x mass perturbations anywhere in the domain during the 2 weeks in March 2010. Similar to the previous plots, these figures do not indicate where the ozone changes due to the NO_x perturbation are occurring; instead they indicate how zonal NO_x perturbations at different altitudes affect the aggregate O_x at each respective altitude band. The sign of this sensitivity reverses between the two altitude bands, with NO_x perturbations leading to increases in O_x in the lower (10–20 km) region through well-known “smog” chemistry but decreases in O_x at higher (20–30 km) altitudes via NO_x -catalyzed ozone destruction. The role of tropical convection is captured in the 10–20 km O_x region, as emissions of NO_x even near the surface can lead to increases in the 10–20 km O_x mass. While some atmospheric dynamics effects (or the onset thereof) are captured in the 10–20 km sensitivities, no clear (i.e., external to the

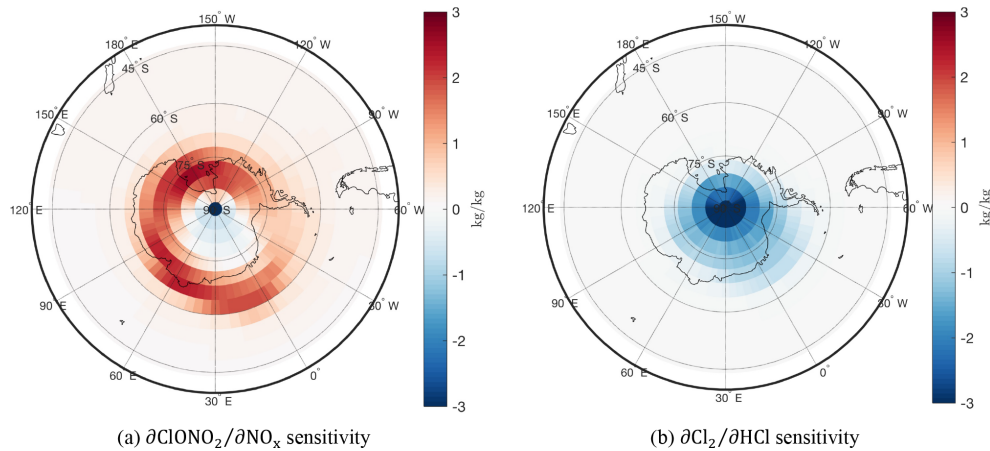


Figure 7. Antarctic chlorine activation (a) and deactivation (b) adjoint sensitivities for a 2-week September simulation at a stratospheric vertical model layer (~ 21 km).

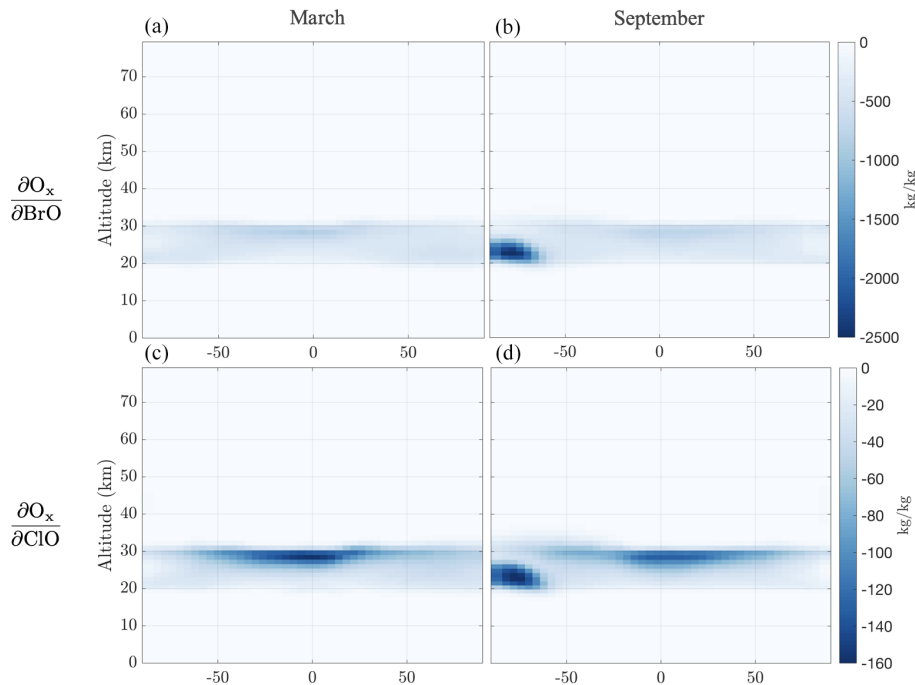


Figure 8. Zonal sensitivities of aggregate O_x at a stratospheric altitude band between 20 and 30 km with respect to perturbations in BrO (a, b) and ClO (c, d) mass in all domain altitudes for a 2-week simulation. Panels (a) and (c) present these for 1–15 March and (b) and (d) for 1–15 of September.

20–30 km region) effects are present in the 20–30 km region in this 2-week simulation, reflecting the different transport timelines in the various regions of the atmosphere. Finally, the sign reversal of the sensitivity at different altitude bands implies the expected existence of an ozone-neutral sensitivity regime, at which level the emissions of NO_x perturbations would have a net zero effect on stratospheric ozone. However, multiyear-long simulations would be required to capture the full tropospheric–stratospheric interactions, including the different transport timescales at different regions of

the atmosphere (Fritz et al., 2022). The $\partial O_x / \partial NO_x$ sensitivity at additional altitude bands is described in Sect. S3 in the Supplement.

5 Summary and conclusions

Sensitivity analyses are widely used in quantifying source–receptor (or source–effect) relationships and further applied in gradient-based assimilation and optimization. Strato-

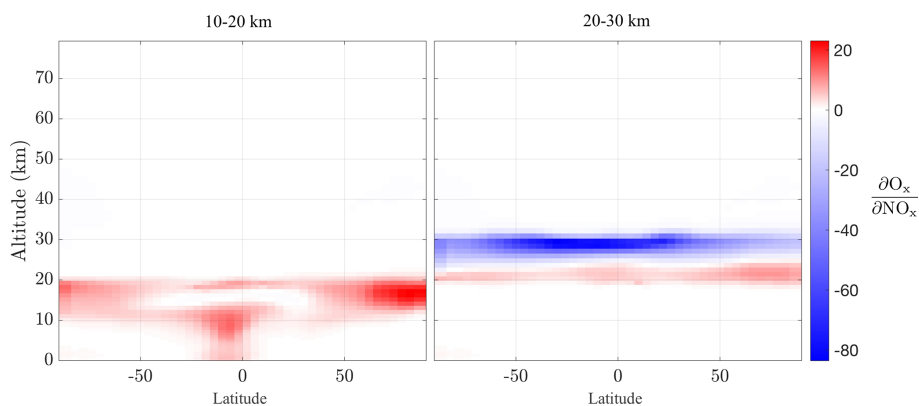


Figure 9. Zonal sensitivities of aggregate O_x at two stratospheric altitude bands (10–20 and 20–30 km) with respect to perturbations in NO_x mass in all domain altitudes in $kg\ kg^{-1}$ for a 2-week simulation in March.

spheric sensitivities can be used to enhance the understanding of underlying chemistry and physics from a new perspective and provide insight on how emissions or other atmospheric changes may lead to ozone depletion. Obtaining sensitivities to all parameters using traditional modeling approaches is computationally intractable. Adjoint, receptor-oriented sensitivities overcome this computational cost, under the assumption that the number of sources of interest is significantly greater than the number of receptors.

This work describes the development of the adjoint of the global GEOS-Chem unified tropospheric–stratospheric chemistry extension (UCX) CTM, which extends the tropospheric capabilities of the GEOS-Chem adjoint (prior to v36) to include stratospheric chemistry. The adjoint model is validated against finite difference tests of the forward component model. We apply the GEOS-Chem UCX adjoint model to calculate short-term stratospheric ozone receptor-oriented sensitivities to ozone (production and loss) precursors. We quantify the Antarctic ozone-depleting potential of BrO, ClO, Cl, and NO_x , as well as the altitude dependence of the NO_x to O_x production–loss relationship.

In this paper we use stratospheric O_x to demonstrate the capabilities of the model in providing a new perspective for examining the underlying chemical and physical processes in a receptor-oriented way. However, sensitivities of any tracer to model parameters can be computed. As such, the adjoint of the GEOS-Chem UCX can be applied to assess the impacts of, including but not limited to, volcanic emissions, changes in water vapor, and stratospheric–tropospheric exchanges. Additionally, besides the largely chemistry-driven phenomena captured in the 2-week sensitivities presented in this work, longer runs would yield insight on the coupled transport and chemistry phenomena. Longer-term sensitivities would also capture the ozone layer impacts of ground-level emissions perturbations. The adjoint of GEOS-Chem UCX also enables the assimilation of observations in an inverse modeling framework and thus the potential for addressing a wide range of scientific questions.

Code and data availability. The source code for GEOS-Chem adjoint model v36 is openly available, and instructions about accessing the code and the required inputs can be found at https://wiki.seas.harvard.edu/geos-chem/index.php/GEOS-Chem_Adjoint (last access: 16 July 2024). This model development and application is undertaken in GEOS-Chem adjoint version v35f (available at: <https://doi.org/10.5281/zenodo.4300535>, Dedoussi et al., 2024) and incorporated in the openly available GEOS-Chem adjoint v36. More details on the GEOS-Chem adjoint versions can be found here: http://wiki.seas.harvard.edu/geos-chem/index.php/GEOS-Chem_Adjoint#Current_GEOS-Chem_adjoint_version_released (last access: 16 July 2024).

Supplement. The supplement related to this article is available online at: <https://doi.org/10.5194/gmd-17-5689-2024-supplement>.

Author contributions. Conceptualization: SRHB; funding acquisition: SRHB; investigation: ICD, DKH, SDE, RLS, SRHB; methodology: ICD, DKH; project administration: RLS, SDE, SRHB; software: ICD, DKH; supervision: SRHB; visualization: ICD; writing (original draft): ICD; writing (review and editing): all.

Competing interests. The contact author has declared that none of the authors has any competing interests.

Disclaimer. Publisher’s note: Copernicus Publications remains neutral with regard to jurisdictional claims made in the text, published maps, institutional affiliations, or any other geographical representation in this paper. While Copernicus Publications makes every effort to include appropriate place names, the final responsibility lies with the authors.

Acknowledgements. We thank Susan Solomon for helpful discussions.

Financial support. This research has been supported by the National Aeronautics and Space Administration (grant no. NNX14AT22A). Irene C. Dedoussi was in part supported through the MIT Martin Family Fellowship for Sustainability.

Review statement. This paper was edited by Havala Pye and reviewed by two anonymous referees.

References

- Ball, W. T., Alsing, J., Mortlock, D. J., Staehelin, J., Haigh, J. D., Peter, T., Tummon, F., Stübi, R., Stenke, A., Anderson, J., Bourassa, A., Davis, S. M., Degenstein, D., Frith, S., Froidevaux, L., Roth, C., Sofieva, V., Wang, R., Wild, J., Yu, P., Ziemke, J. R., and Rozanov, E. V.: Evidence for a continuous decline in lower stratospheric ozone offsetting ozone layer recovery, *Atmos. Chem. Phys.*, 18, 1379–1394, <https://doi.org/10.5194/acp-18-1379-2018>, 2018.
- Bey, I., Jacob, D. J., Yantosca, R. M., Logan, J. A., Field, B. D., Fiore, A. M., Li, Q., Liu, H. Y., Mickley, L. J., and Schultz, M. G.: Global modeling of tropospheric chemistry with assimilated meteorology: Model description and evaluation, *J. Geophys. Res.*, 106, 23073–23095, <https://doi.org/10.1029/2001JD000807>, 2001.
- Bian, H. and Prather, M. J.: Fast-J2: Accurate Simulation of Stratospheric Photolysis in Global Chemical Models, *J. Atmos. Chem.*, 41, 281–296, <https://doi.org/10.1023/A:1014980619462>, 2002.
- Brasseur, G. P., Cox, R. A., Hauglustaine, D., Isaksen, I., Lelieveld, J., Lister, D. H., Sausen, R., Schumann, U., Wahner, A., and Wiesen, P.: European scientific assessment of the atmospheric effects of aircraft emissions, *Atmos. Environ.*, 32, 2329–2418, [https://doi.org/10.1016/S1352-2310\(97\)00486-X](https://doi.org/10.1016/S1352-2310(97)00486-X), 1998.
- Butchart, N.: The Brewer-Dobson circulation, *Rev. Geophys.*, 52, 157–184, <https://doi.org/10.1002/2013RG000448>, 2014.
- Capps, S. L., Henze, D. K., Hakami, A., Russell, A. G., and Nenes, A.: ANISORROPIA: the adjoint of the aerosol thermodynamic model ISORROPIA, *Atmos. Chem. Phys.*, 12, 527–543, <https://doi.org/10.5194/acp-12-527-2012>, 2012.
- Chipperfield, M. P., Cariolle, D., and Simon, P.: A 3D transport model study of chlorine activation during EASOE, *Geophys. Res. Lett.*, 21, 1467–1470, <https://doi.org/10.1029/93GL01679>, 1994.
- Clappier, A., Belis, C. A., Pernigotti, D., and Thunis, P.: Source apportionment and sensitivity analysis: two methodologies with two different purposes, *Geosci. Model Dev.*, 10, 4245–4256, <https://doi.org/10.5194/gmd-10-4245-2017>, 2017.
- Considine, D. B., Douglass, A. R., Connell, P. S., Kinnison, D. E., and Rotman, D. A.: A polar stratospheric cloud parameterization for the global modeling initiative three-dimensional model and its response to stratospheric aircraft, *J. Geophys. Res.-Atmos.*, 105, 3955–3973, <https://doi.org/10.1029/1999JD900932>, 2000.
- Crutzen, P. J.: The influence of nitrogen oxides on the atmospheric ozone content, *Q. J. Roy. Meteor. Soc.*, 96, 320–325, <https://doi.org/10.1002/qj.49709640815>, 1970.
- Cunnold, D. M., Aleya, F. N., and Prinn, R. G.: Relative effects on atmospheric ozone of latitude and altitude of supersonic flight, 15, 337–345, <https://doi.org/10.2514/3.7327>, 1977.
- Daescu, D. N., Sandu, A., and Carmichael, G. R.: Direct and adjoint sensitivity analysis of chemical kinetic systems with KPP: II – Numerical validation and applications, *Atmos. Environ.*, 37, 5097–5114, <https://doi.org/10.1016/j.atmosenv.2003.08.020>, 2003.
- Damian, V., Sandu, A., Damian, M., Potra, F., and Carmichael, G. R.: The kinetic preprocessor KPP—a software environment for solving chemical kinetics, *Comput. Chem. Eng.*, 26, 1567–1579, [https://doi.org/10.1016/S0098-1354\(02\)00128-X](https://doi.org/10.1016/S0098-1354(02)00128-X), 2002.
- Daniel, J. S., Solomon, S., Portmann, R. W., and Garcia, R. R.: Stratospheric ozone destruction: The importance of bromine relative to chlorine, *J. Geophys. Res.-Atmos.*, 104, 23871–23880, <https://doi.org/10.1029/1999JD900381>, 1999.
- Dedoussi, I. C., Eastham, S. D., Monier, E., and Barrett, S. R. H.: Premature mortality related to United States cross-state air pollution, *Nature*, 578, 261–265, <https://doi.org/10.1038/s41586-020-1983-8>, 2020.
- Dedoussi, I. C., Henze, D. K., Eastham, S. D., Speth, R. L., and Barrett, S. R. H.: GEOS-Chem UCX adjoint model code (v35f), Zenodo [code], <https://doi.org/10.5281/zenodo.4300535>, 2024.
- Eastham, S. D. and Barrett, S. R. H.: Aviation-attributable ozone as a driver for changes in mortality related to air quality and skin cancer, *Atmos. Environ.*, 144, 17–23, <https://doi.org/10.1016/j.atmosenv.2016.08.040>, 2016.
- Eastham, S. D., Weisenstein, D. K., and Barrett, S. R. H.: Development and evaluation of the unified tropospheric-stratospheric chemistry extension (UCX) for the global chemistry-transport model GEOS-Chem, *Atmos. Environ.*, 89, 52–63, <https://doi.org/10.1016/j.atmosenv.2014.02.001>, 2014.
- Eastham, S. D., Keith, D. W., and Barrett, S. R. H.: Mortality tradeoff between air quality and skin cancer from changes in stratospheric ozone, *Environ. Res. Lett.*, 13, 034035, <https://doi.org/10.1088/1748-9326/aaad2e>, 2018.
- Eastham, S. D., Fritz, T., Sanz-Morère, I., Prashanth, P., Allroggen, F., Prinn, R. G., Speth, R. L., and Barrett, S. R. H.: Impacts of a near-future supersonic aircraft fleet on atmospheric composition and climate, *Environ. Sci. Atmos.*, 2, 388–403, <https://doi.org/10.1039/D1EA00081K>, 2022.
- Emmons, L. K., Hess, P. G., Lamarque, J.-F., and Pfister, G. G.: Tagged ozone mechanism for MOZART-4, CAM-chem and other chemical transport models, *Geosci. Model Dev.*, 5, 1531–1542, <https://doi.org/10.5194/gmd-5-1531-2012>, 2012.
- Farman, J. C., Gardiner, B. G., and Shanklin, J. D.: Large losses of total ozone in Antarctica reveal seasonal ClO_x/NO_x interaction, *Nature*, 315, 207–210, <https://doi.org/10.1038/315207a0>, 1985.
- Fritz, T. M., Dedoussi, I. C., Eastham, S. D., Speth, R. L., Henze, D. K., and Barrett, S. R. H.: Identifying the ozone-neutral aircraft cruise altitude, *Atmos. Environ.*, 276, 119057, <https://doi.org/10.1016/j.atmosenv.2022.119057>, 2022.
- Giering, R. and Kaminski, T.: Recipes for adjoint code construction, *ACM T. Math. Software*, 24, 437–474, <https://doi.org/10.1145/293686.293695>, 1998.
- Giles, M. B. and Pierce, N. A.: An introduction to the adjoint approach to design, *Flow, Turbulence and Combustion*, 65, 393–415, <https://doi.org/10.1023/A:1011430410075>, 2000.
- Greenlade, J. W., Alexander, S. P., Schofield, R., Fisher, J. A., and Klekociuk, A. K.: Stratospheric ozone intrusion events and their impacts on tropospheric ozone in the South-

- ern Hemisphere, *Atmos. Chem. Phys.*, 17, 10269–10290, <https://doi.org/10.5194/acp-17-10269-2017>, 2017.
- Gu, Y., Henze, D. K., Nawaz, M. O., Cao, H., and Wagner, U. J.: Sources of PM_{2.5}-Associated Health Risks in Europe and Corresponding Emission-Induced Changes During 2005–2015, *GeoHealth*, 7, e2022GH000767, <https://doi.org/10.1029/2022GH000767>, 2023.
- Hakami, A., Henze, D. K., Seinfeld, J. H., Singh, K., Sandu, A., Kim, S., Byun, D., and Li, Q.: The adjoint of CMAQ, *Environmental Science and Technology*, 41, 7807–7817, <https://doi.org/10.1021/es070944p>, 2007.
- Hascoet, L. and Pascual, V.: The Tapenade Automatic Differentiation Tool: Principles, Model, and Specification, *ACM Trans. Math. Softw.*, 39, 20, <https://doi.org/10.1145/2450153.2450158>, 2013.
- Henze, D. K., Hakami, A., and Seinfeld, J. H.: Development of the adjoint of GEOS-Chem, *Atmos. Chem. Phys.*, 7, 2413–2433, <https://doi.org/10.5194/acp-7-2413-2007>, 2007.
- Henze, D. K., Seinfeld, J. H., and Shindell, D. T.: Inverse modeling and mapping US air quality influences of inorganic PM_{2.5} precursor emissions using the adjoint of GEOS-Chem, *Atmos. Chem. Phys.*, 9, 5877–5903, <https://doi.org/10.5194/acp-9-5877-2009>, 2009.
- Hossaini, R., Chipperfield, M. P., Montzka, S. A., Rap, A., Dhomse, S., and Feng, W.: Efficiency of short-lived halogens at influencing climate through depletion of stratospheric ozone, *Nat. Geosci.*, 8, 186–190, <https://doi.org/10.1038/ngeo2363>, 2015.
- Hossaini, R., Chipperfield, M. P., Montzka, S. A., Leeson, A. A., Dhomse, S. S., and Pyle, J. A.: The increasing threat to stratospheric ozone from dichloromethane, *Nat. Commun.*, 8, 15962, <https://doi.org/10.1038/ncomms15962>, 2017.
- Huijnen, V., Williams, J., van Weele, M., van Noije, T., Krol, M., Dentener, F., Segers, A., Houweling, S., Peters, W., de Laat, J., Boersma, F., Bergamaschi, P., van Velthoven, P., Le Sager, P., Eskes, H., Alkemade, F., Scheele, R., Nédélec, P., and Pätz, H.-W.: The global chemistry transport model TM5: description and evaluation of the tropospheric chemistry version 3.0, *Geosci. Model Dev.*, 3, 445–473, <https://doi.org/10.5194/gmd-3-445-2010>, 2010.
- Jaeglé, L., Webster, C. R., May, R. D., Scott, D. C., Stimpfle, R. M., Kohn, D. W., Wennberg, P. O., Hanisco, T. F., Cohen, R. C., Proffitt, M. H., Kelly, K. K., Elkins, J., Baumgardner, D., Dye, J. E., Wilson, J. C., Poeschel, R. F., Chan, K. R., Salawitch, R. J., Tuck, A. F., Hovde, S. J., and Yung, Y. L.: Evolution and stoichiometry of heterogeneous processing in the Antarctic stratosphere, *J. Geophys. Res.-Atmos.*, 102, 13235–13253, <https://doi.org/10.1029/97JD00935>, 1997.
- Johnston, H.: Reduction of stratospheric ozone by nitrogen oxide catalysts from supersonic transport exhaust, *Science*, 173, 517–522, <https://doi.org/10.1126/science.173.3996.517>, 1971.
- Kinnison, D. E., Brasseur, G. P., Walters, S., Garcia, R. R., Marsh, D. R., Sassi, F., Harvey, V. L., Randall, C. E., Emmons, L., Lamarque, J. F., Hess, P., Orlando, J. J., Tie, X. X., Randel, W., Pan, L. L., Gettelman, A., Granier, C., Diehl, T., Niemeier, U., and Simmons, A. J.: Sensitivity of chemical tracers to meteorological parameters in the MOZART-3 chemical transport model, *J. Geophys. Res.-Atmos.*, 112, D20302, <https://doi.org/10.1029/2006JD007879>, 2007.
- Köhler, M. O., Rädcl, G., Dessens, O., Shine, K. P., Rogers, H. L., Wild, O., and Pyle, J. A.: Impact of perturbations to nitrogen oxide emissions from global aviation, *J. Geophys. Res.-Atmos.*, 113, D11305, <https://doi.org/10.1029/2007JD009140>, 2008.
- Kopacz, M., Jacob, D. J., Fisher, J. A., Logan, J. A., Zhang, L., Megretskaia, I. A., Yantosca, R. M., Singh, K., Henze, D. K., Burrows, J. P., Buchwitz, M., Khlystova, I., McMillan, W. W., Gille, J. C., Edwards, D. P., Eldering, A., Thouret, V., and Nedelec, P.: Global estimates of CO sources with high resolution by adjoint inversion of multiple satellite datasets (MOPITT, AIRS, SCIAMACHY, TES), *Atmos. Chem. Phys.*, 10, 855–876, <https://doi.org/10.5194/acp-10-855-2010>, 2010.
- Kuttippurath, J. and Nair, P. J.: The signs of Antarctic ozone hole recovery, *Scientific Reports*, 7, 585, <https://doi.org/10.1038/s41598-017-00722-7>, 2017.
- Lickley, M., Solomon, S., Fletcher, S., Velders, G. J. M., Daniel, J., Rigby, M., Montzka, S. A., Kuijpers, L. J. M., and Stone, K.: Quantifying contributions of chlorofluorocarbon banks to emissions and impacts on the ozone layer and climate, *Nat. Commun.*, 11, 1380, <https://doi.org/10.1038/s41467-020-15162-7>, 2020.
- Maruhashi, J., Grewe, V., Frömming, C., Jöckel, P., and Dedoussi, I. C.: Transport patterns of global aviation NO_x and their short-term O₃ radiative forcing – a machine learning approach, *Atmos. Chem. Phys.*, 22, 14253–14282, <https://doi.org/10.5194/acp-22-14253-2022>, 2022.
- McElroy, M. B., Salawitch, R. J., Wofsy, S. C., and Logan, J. A.: Reductions of Antarctic ozone due to synergistic interactions of chlorine and bromine, *Nature*, 321, 759–762, <https://doi.org/10.1038/321759a0>, 1986.
- Molina, M. J. and Rowland, F. S.: Stratospheric sink for chlorofluoromethanes: chlorine atom-catalysed destruction of ozone, *Nature*, 249, 810–812, <https://doi.org/10.1038/249810a0>, 1974.
- Montzka, S. A., Dutton, G. S., Yu, P., Ray, E., Portmann, R. W., Daniel, J. S., Kuijpers, L., Hall, B. D., Mondeel, D., Siso, C., Nance, J. D., Rigby, M., Manning, A. J., Hu, L., Moore, F., Miller, B. R., and Elkins, J. W.: An unexpected and persistent increase in global emissions of ozone-depleting CFC-11, *Nature*, 557, 413–417, <https://doi.org/10.1038/s41586-018-0106-2>, 2018.
- Murray, L. T., Jacob, D. J., Logan, J. A., Hudman, R. C., and Koshak, W. J.: Optimized regional and interannual variability of lightning in a global chemical transport model constrained by LIS/OTD satellite data, *J. Geophys. Res.-Atmos.*, 117, D20307, <https://doi.org/10.1029/2012JD017934>, 2012.
- NASA Ozone Watch: NASA Ozone Watch: Images, data, and information for atmospheric ozone, https://ozonewatch.gsfc.nasa.gov/meteorology/ozone_2009_MERRA_NH.html, last access: 25 March 2018.
- Nawaz, M. O., Henze, D. K., Anenberg, S. C., Braun, C., Miller, J., and Pronk, E.: A Source Apportionment and Emission Scenario Assessment of PM_{2.5}- and O₃-Related Health Impacts in G20 Countries, *GeoHealth*, 7, e2022GH000713, <https://doi.org/10.1029/2022GH000713>, 2023.
- Qu, Z., Henze, D. K., Cooper, O. R., and Neu, J. L.: Impacts of global NO_x inversions on NO₂ and ozone simulations, *Atmos. Chem. Phys.*, 20, 13109–13130, <https://doi.org/10.5194/acp-20-13109-2020>, 2020.
- Quadros, F., Snellen, M., and Dedoussi, I. C.: Regional sensitivities of air quality and human health impacts to aviation emissions,

- Environ. Res. Lett., 15, 105013, <https://doi.org/10.1088/1748-9326/abb2c5>, 2020.
- Rigby, M., Park, S., Saito, T., Western, L. M., Redington, A. L., Fang, X., Henne, S., Manning, A. J., Prinn, R. G., Dutton, G. S., Fraser, P. J., Ganesan, A. L., Hall, B. D., Harth, C. M., Kim, J., Kim, K.-R., Krummel, P. B., Lee, T., Li, S., Liang, Q., Lunt, M. F., Montzka, S. A., Mühle, J., O'Doherty, S., Park, M.-K., Reimann, S., Salameh, P. K., Simmonds, P., Tunnicliffe, R. L., Weiss, R. F., Yokouchi, Y., and Young, D.: Increase in CFC-11 emissions from eastern China based on atmospheric observations, *Nature*, 569, 546–550, <https://doi.org/10.1038/s41586-019-1193-4>, 2019.
- Ross, M., Toohey, D., Peinemann, M., and Ross, P.: Limits on the space launch market related to stratospheric ozone depletion, *Astropolitics*, 7, 50–82, <https://doi.org/10.1080/14777620902768867>, 2009.
- Rotman, D. A., Tannahill, J. R., Kinnison, D. E., Connell, P. S., Bergmann, D., Proctor, D., Rodriguez, J. M., Lin, S. J., Rood, R. B., Prather, M. J., Rasch, P. J., Considine, D. B., Ramarosan, R., and Kawa, S. R.: Global Modeling Initiative assessment model: Model description, integration, and testing of the transport shell, *J. Geophys. Res.-Atmos.*, 106, 1669–1691, <https://doi.org/10.1029/2000JD900463>, 2001.
- Ryan, R. G., Marais, E. A., Balhatchet, C. J., and Eastham, S. D.: Impact of Rocket Launch and Space Debris Air Pollutant Emissions on Stratospheric Ozone and Global Climate, *Earth's Future*, 10, e2021EF002612, <https://doi.org/10.1029/2021EF002612>, 2022.
- Sander, S. P., Friedl, R. R., DeMore, W. B., Ravishankara, A. R., Golden, D. M., Kolb, C. E., Kurylo, M. J., Hampson, R. F., Huie, R. E., Molina, M. J., and Moortgat, G. K.: Chemical Kinetics and Photochemical Data for Use in Stratospheric Modeling; Supplement to Evaluation 12: Update of Key Reactions, https://jpldataeval.jpl.nasa.gov/pdf/JPL_00-03.pdf (last access: 22 July 2024), 2000.
- Sander, S. P., Friedl, R. R., Golden, D. M., Kurylo, M. J., Moortgat, G. K., Wine, P. H., Ravishankara, a R., Kolb, C. E., Molina, M. J., Diego, S., Jolla, L., Huie, R. E., and Orkin, V. L.: Chemical Kinetics and Photochemical Data for Use in Atmospheric Studies, Evaluation No. 17, JPL Publication 10-6, Pasadena, <https://jpldataeval.jpl.nasa.gov/pdf/JPL10-6Final15June2011.pdf> (last access: 22 July 2024), 2011.
- Sandu, A., Daescu, D. N., and Carmichael, G. R.: Direct and adjoint sensitivity analysis of chemical kinetic systems with KPP: Part I – Theory and software tools, *Atmos. Environ.*, 37, 5083–5096, <https://doi.org/10.1016/j.atmosenv.2003.08.019>, 2003.
- Sandu, A., Daescu, D. N., Carmichael, G. R., and Chai, T.: Adjoint sensitivity analysis of regional air quality models, *J. Comput. Phys.*, 204, 222–252, <https://doi.org/10.1016/j.jcp.2004.10.011>, 2005.
- Sausen, R., Deckert, R., Jöckel, P., Aquila, V., Brinkop, S., Burkhardt, U., Cionni, I., Dall'Amico, M., Dameris, M., Dietmüller, S., Eyring, V., Gottschaldt, K., Grewe, V., Hendricks, J., Ponater, M., and Righi, M.: Global Chemistry-Climate Modelling with EMAC BT – High Performance Computing in Science and Engineering, Garching/Munich 2009, 663–674, <https://doi.org/10.1007/978-3-642-13872-0>, 2010.
- Schäfer, A., Heywood, J. B., Jacoby, H. D., and Waitz, I. A.: Transportation in a Climate-Constrained World, The MIT Press, ISBN 9780262512343, 2009.
- Sherwen, T., Schmidt, J. A., Evans, M. J., Carpenter, L. J., Großmann, K., Eastham, S. D., Jacob, D. J., Dix, B., Koenig, T. K., Sinreich, R., Ortega, I., Volkamer, R., Saiz-Lopez, A., Prados-Roman, C., Mahajan, A. S., and Ordóñez, C.: Global impacts of tropospheric halogens (Cl, Br, I) on oxidants and composition in GEOS-Chem, *Atmos. Chem. Phys.*, 16, 12239–12271, <https://doi.org/10.5194/acp-16-12239-2016>, 2016.
- Singh, K., Eller, P., Sandu, A., Bowman, K., Jones, D., and Lee, M.: Improving GEOS-Chem Model Tropospheric Ozone through Assimilation of Pseudo Tropospheric Emission Spectrometer Profile Retrievals, in: Computational Science – ICCS 2009, ICCS 2009, Lecture Notes in Computer Science, vol. 5545, edited by: Allen, G., Nabrzyski, J., Seidel, E., van Albada, G. D., Dongarra, J., and Sloot, P. M. A., Springer, Berlin, Heidelberg, https://doi.org/10.1007/978-3-642-01973-9_34, 2009.
- Slaper, H., Velders, G. J. M., Daniel, J. S., de Gruijl, F. R., and van der Leun, J. C.: Estimates of ozone depletion and skin cancer incidence to examine the Vienna Convention achievements, *Nature*, 384, 256, <https://doi.org/10.1038/384256a0>, 1996.
- Solomon, S.: Stratospheric ozone depletion: A review of concepts and history, *Rev. Geophys.*, 37, 275–316, <https://doi.org/10.1029/1999RG900008>, 1999.
- Solomon, S., Garcia, R. R., Rowland, F. S., and Wuebbles, D. J.: On the depletion of Antarctic ozone, *Nature*, 321, 755–758, <https://doi.org/10.1038/321755a0>, 1986.
- Solomon, S., Kinnison, D., Bandoro, J., and Garcia, R.: Simulation of polar ozone depletion: An update, *J. Geophys. Res.-Atmos.*, 120, 7958–7974, <https://doi.org/10.1002/2015JD023365>, 2015.
- Solomon, S., Ivy, D. J., Kinnison, D., Mills, M. J., Neely, R. R., and Schmidt, A.: Emergence of healing in the Antarctic ozone layer, *Science*, 353, 269–274, <https://doi.org/10.1126/science.aae0061>, 2016.
- Søvde, O. A., Prather, M. J., Isaksen, I. S. A., Berntsen, T. K., Stordal, F., Zhu, X., Holmes, C. D., and Hsu, J.: The chemical transport model Oslo CTM3, *Geosci. Model Dev.*, 5, 1441–1469, <https://doi.org/10.5194/gmd-5-1441-2012>, 2012.
- Tang, Z., Jiang, Z., Chen, J., Yang, P., and Shen, Y.: The capabilities of the adjoint of GEOS-Chem model to support HEMCO emission inventories and MERRA-2 meteorological data, *Geosci. Model Dev.*, 16, 6377–6392, <https://doi.org/10.5194/gmd-16-6377-2023>, 2023.
- Toon, G. C., Farmer, C. B., Lowes, L. L., Schaper, P. W., Blavier, J.-F., and Norton, R. H.: Infrared aircraft measurements of stratospheric composition over Antarctica during September 1987, *J. Geophys. Res.-Atmos.*, 94, 16571–16596, <https://doi.org/10.1029/JD094iD14p16571>, 1989.
- Wang, J., Xu, X., Henze, D. K., Zeng, J., Ji, Q., Tsay, S.-C., and Huang, J.: Top-down estimate of dust emissions through integration of MODIS and MISR aerosol retrievals with the GEOS-Chem adjoint model, *Geophys. Res. Lett.*, 39, L08802, <https://doi.org/10.1029/2012GL051136>, 2012.
- Wang, X., Jacob, D. J., Eastham, S. D., Sulprizio, M. P., Zhu, L., Chen, Q., Alexander, B., Sherwen, T., Evans, M. J., Lee, B. H., Haskins, J. D., Lopez-Hilfiker, F. D., Thornton, J. A., Huey, G. L., and Liao, H.: The role of chlorine in global

- tropospheric chemistry, *Atmos. Chem. Phys.*, 19, 3981–4003, <https://doi.org/10.5194/acp-19-3981-2019>, 2019.
- Weatherhead, E. C. and Andersen, S. B.: The search for signs of recovery of the ozone layer, *Nature*, 441, 39–45, <https://doi.org/10.1038/nature04746>, 2006.
- Weber, M., Coldewey-Egbers, M., Fioletov, V. E., Frith, S. M., Wild, J. D., Burrows, J. P., Long, C. S., and Loyola, D.: Total ozone trends from 1979 to 2016 derived from five merged observational datasets – the emergence into ozone recovery, *Atmos. Chem. Phys.*, 18, 2097–2117, <https://doi.org/10.5194/acp-18-2097-2018>, 2018.
- Weisenstein, D. K., Yue, G. K., Ko, M. K. W., Sze, N.-D., Rodriguez, J. M., and Scott, C. J.: A two-dimensional model of sulfur species and aerosols, *J. Geophys. Res.-Atmos.*, 102, 13019–13035, <https://doi.org/10.1029/97JD00901>, 1997.
- WMO/UNEP: World Meteorological Organization/United Nations Environment Programme Scientific Assessment of Ozone Depletion: 2014, <https://csl.noaa.gov/assessments/ozone/2014/report/2014OzoneAssessment.pdf> (last access: 22 July 2024), 2014.
- Zhao, S., Russell, M. G., Hakami, A., Capps, S. L., Turner, M. D., Henze, D. K., Percell, P. B., Resler, J., Shen, H., Russell, A. G., Nenes, A., Pappin, A. J., Napelenok, S. L., Bash, J. O., Fahey, K. M., Carmichael, G. R., Stanier, C. O., and Chai, T.: A multiphase CMAQ version 5.0 adjoint, *Geosci. Model Dev.*, 13, 2925–2944, <https://doi.org/10.5194/gmd-13-2925-2020>, 2020.
- Zhu, L., Jacob, D. J., Eastham, S. D., Sulprizio, M. P., Wang, X., Sherwen, T., Evans, M. J., Chen, Q., Alexander, B., Koenig, T. K., Volkamer, R., Huey, L. G., Le Breton, M., Bannan, T. J., and Percival, C. J.: Effect of sea salt aerosol on tropospheric bromine chemistry, *Atmos. Chem. Phys.*, 19, 6497–6507, <https://doi.org/10.5194/acp-19-6497-2019>, 2019.